Int. J. Heat Mass Transfer. Vol. 35, No. 9, pp. 2087–2099, 1992
Printed in Great Britain

0017–9310/92 $5.00 + 0.00

Analysis of flow and heat transfer characteristics of an asymmetrical flat plate heat pipe

K. VAFAI and W. WANG
Department of Mechanical Engineering, The Ohio State University, Columbus, OH 43210-1107, U.S.A.

(*Received* 3 *July* 1991 *and in final form* 11 *September* 1991)

Abstract—An in-depth integral analysis revealing various physical aspects of an asymmetrical flat plate heat pipe is presented in this work. The resulting psuedo-three-dimensional vapor phase flow field is bifurcated on the x–y plane due to the asymmetrical nature of the heat source and sinks. The analytical results for the shifted vapor velocity profiles on the x–y plane, the overall axial pressure distributions in both vapor and liquid phases and the axial vapor temperature distribution in the heat pipe are obtained. There is good qualitative agreement between the present results and those based on the solution of the field equations for the conventional symmetrical case. The analysis provides accurate analytical expressions for velocity and pressure distributions for this type of non-conventional heat pipe.

1. INTRODUCTION

HEAT PIPES have been widely used in heat transfer related applications for nearly 30 years. Theoretical and practical research aspects concerning the transport mechanism, the structure of the container, wick and materials used in the heat pipe have been well established for many applications, such as spacecraft thermal control, electronic systems cooling and many commercial thermal devices. The fluid flow within a heat pipe dealing with the vapor flow in the core region and condensate flow in the wick is an important topic in most of these research studies. Most of the investigators have concentrated on the study of conventional heat pipes, which have a symmetrical heat source and sink. The finite difference method has been extensively employed to solve the governing differential equations in the vapor phase for such cases [1–4]. But, the asymmetrical characteristics of a heat pipe have been mostly neglected.

A comprehensive review of the physical phenomena and applications of heat pipes is given by Tien [5] and Winter and Barsch [6]. Tien and Rohani [1] have presented the numerical results displaying vapor pressure distributions and heat pipe performance for axisymmetrical heat pipes, and general trends for pressure drop in the evaporator section and pressure recovery in the condenser section. Further numerical results, including the pressure and velocity distributions, were reported by Narayana [2], pointing out that an increase in suction rate in the condenser section produces a vapor flow reversal. Faghri [3] has presented his results for a double-walled concentric heat pipe which indicate that the pressure distribution and velocity profile for a double-walled concentric heat pipe are almost the same as a conventional heat pipe. There have been several analytical and experimental studies of the heat pipe phenomena. For example, Udell [7] reported analytical and experimental studies for a one-dimensional, steady state problem on the heat pipe effect in porous media. In the model developed, gravity forces, capillarity and change of phase were considered. Leverett correlation relating capillary pressure to permeability, porosity and surface tension was also used in this study. Relative permeability correlations found by Fatt and Klikoff [8] were also employed. Udell and Fitch [9] reported a further study considering the effects of non-condensible gases. In their work, the effect of non-condensible gases on Kelvin's equation is explained and utilized.

In this work, a detailed analysis of the intra-wick interactions and integral solutions for the velocity and pressure fields within the flat plate heat pipe are presented for the first time. The integral analysis is employed to investigate the vapor and liquid flow in a flat plate heat pipe heated asymmetrically. The resulting psuedo-three-dimensional vapor phase flow field and the bifurcation phenomena on the x–y plane due to the asymmetrical nature of the heat source and sinks have been vividly illustrated and the analytical results for the shifted vapor velocity profiles on the x–y plane, the overall axial pressure distributions in both vapor and liquid phases and the axial vapor temperature distribution in the heat pipe are obtained.

A specific application will be considered for the flat plate heat pipe used in our analysis, namely Boron Neutron Capture Therapy (BNCT). For this application, the protons which are accelerated by an accelerator bombard a lithium target to produce the neutrons which are used for treatment of brain tumors. The flat plate heat pipe configuration will then be used for removing a high heat flux generated as a result of proton bombardments of the lithium target. The flat plate heat pipe will be used as an effective heat sink as well as an additional moderator for the neutron

NOMENCLATURE

A_e	evaporator area [m^2]
b	half width of any of the vapor channels [m]
$f(x)$	position of maximum value of vapor velocity in y direction [m]
$f^+(x^+)$	dimensionless position of the maximum vapor velocity in y^+ direction
h	height of vapor space for the heat pipe [m]
h_{Li}	thickness of the lithium disk [m]
h_{wall}	thickness of the heat pipe wall [m]
h_w	thickness of the wick [m]
h_b^+	dimensionless half width of any of the vapor channels, b/h
h_w^+	dimensionless thickness of the wick, h_w/h
h_{fg}	latent heat of working fluid [kJ kg^{-1}]
k_{Li}	thermal conductivity of the lithium [W m^{-1} °C^{-1}]
k_w	thermal conductivity of the wick [W m^{-1} °C^{-1}]
k_{wall}	thermal conductivity of the heat pipe wall [W m^{-1} °C^{-1}]
K	permeability [m^2]
K^+	dimensionless permeability, K/h_w^2
l	length of the heat pipe [m]
l^+	dimensionless length of the heat pipe
l_b	width of the heat pipe [m]
l_e	length of the evaporator [m]
p_l	liquid pressure [Pa]
p_v	vapor pressure [Pa]
p_l^+	dimensionless liquid pressure, $p_l/\rho_l U_{ol}^2$
p_v^+	dimensionless vapor pressure, $p_v/\rho_v U_{ov}^2$
Δp_{cap}	capillary pressure head generated by the wick [Pa]
Δp_l	overall liquid pressure drop along the heat pipe [Pa]
Δp_{total}	total pressure head in the heat pipe [Pa]
Δp_v	overall vapor pressure drop along the heat pipe [Pa]
Δp_l^+	overall dimensionless liquid pressure drop along the heat pipe, $p_l^+ - p_{ov}^+$
Δp_v^+	overall dimensionless vapor pressure drop along the heat pipe, $p_v^+ - p_{ov}^+$
q_e	imposed heat flux on the evaporator [W m^{-2}]
Q	rate of heat transfer generated by neutron bombardment [W]
r_w	porous radius of wick [m]
Re_h	injection Reynolds number, $v_1 h/\nu_v$
T_{Li}	free surface temperature of the lithium [°C]
T_v	vapor temperature [°C]
T_{ov}^+	dimensionless saturate vapor temperature, $T_{ov}h_{fg}/R$
ΔT_{Li}	temperature drop across the lithium disk [°C]
ΔT_w	temperature drop across the wick [°C]
ΔT_{wall}	temperature drop across the heat pipe wall [°C]
ΔT_v^+	dimensionless vapor temperature drop along the heat pipe, $T^+ - T_{ov}^+$
u_l	liquid velocity [m s^{-1}]
u_v	vapor velocity [m s^{-1}]
u_l^+	dimensionless liquid velocity, u_l/U_{ol}
u_v^+	dimensionless vapor velocity, u_v/U_{ov}
U_{ol}	maximum liquid velocity [m s^{-1}]
U_{ov}	maximum vapor velocity [m s^{-1}]
U_v^+	dimensionless vapor velocity component in x^+ direction
v_1	vapor injection velocity [m s^{-1}]
v_2	vapor suction velocity [m s^{-1}]
v_1^+	dimensionless vapor injection velocity, $v_1 h/\nu_v$
v_2^+	dimensionless vapor suction velocity, $v_2 h/\nu_v$.

Greek letters

μ_l	liquid viscosity [Ns m^{-2}]
μ_v	vapor viscosity [Ns m^{-2}]
μ^+	dimensionless viscosity, μ_v/μ_l
ν_v	kinematic viscosity of vapor [m^2 s^{-1}]
ρ_l	liquid density [kg m^3]
ρ_v	vapor density [kg m^{-3}]
σ_l	surface tension of the heat pipe's working liquid [N m^{-1}]
φ	ratio of the evaporator length to the heat pipe length.

Subscripts

c	condenser
e	evaporator
l	liquid phase
v	vapor phase
w	wick.

Superscript

+	dimensionless quantities.

production. Expressions for the pressure and velocity distributions are obtained and discussed in relation to the BNCT application. Qualitatively, our results compare quite favorably with the results reported by other researchers [10, 11].

The selection of the material which will be used in manufacturing the heat pipe also needs some careful consideration. This is because the interference of the reflected (or outwardly diffused) neutrons (which are produced as a result of the interaction between the

protons and the lithium) with certain materials produces gamma rays which is unacceptable and must be avoided. For this reason heavy water (D_2O) is chosen as the operating fluid for the heat pipe and the heat pipe material itself is chosen to be aluminum. In the present work the heat pipe will be designed such that it would be able to comfortably remove the heat generated as a result of the proton bombardments of the lithium target. Since a large amount of energy falls upon a relatively small area of the lithium surface, we need to ensure that there will not be any flash evaporation. The present analysis clearly shows that it is possible to attain temperatures well below the melting point of the lithium for the high heat flux situation in the BNCT application. This in turn prevents any adverse pressure build up within the system.

2. ANALYSIS AND FORMULATION

The schematic diagram of the heat pipe for the present investigation is shown in Fig. 1(a). It can be seen that the heat pipe is mounted symmetrically under the lithium target area. A cooling jacket is used around the outer periphery of the heat pipe for removing the dissipated heat. Based on our analysis the surface temperature of the heat pipe turns out to be low enough that the fluid inside the cooling jacket can pass through an appropriate cooling loop. This is quite advantageous since it will result in a closed loop system thus further reducing any possibility of an accidental contamination of the surroundings. As shown in Fig. 1(a), the heat generated from the proton bombardment of the lithium is imposed on the upper part, which is then transferred equally to both sides of the heat pipe. The multiple independent vapor flow channels and the coordinate system for the flat plate heat pipe are shown in Figs. 1(b) and (c). The generated heat causes the vaporization and subsequent pressurization of the liquid in the wick. Part of the vapor is condensed on the opposite surface of the evaporator, however, most of it is condensed downstream of the evaporator on both sides of the condenser region.

Obviously, the vapor flow in the heat pipe does not have a symmetrical velocity profile. The location of the maximum vapor velocity will be shifted towards the lower plate due to the vapor injection from the heating side of the upper plate. As the vapor flows downstream, the location of the maximum velocity will gradually shift towards the center line due to the presence of symmetrical cooling conditions. The vapor space is divided into several channels by the vertical wicks which transport liquid from the lower wick to the upper wick. Therefore, the vapor velocity along the longitudinal direction will be a function of the x, y and z directions. The condensate in the upper wick (section 2 of Fig. 2), flows back directly to the evaporator along the wick by capillary force. However, in section 4 of the lower wick, the condensate will move directly along the horizontal wick towards section 3 of the lower wick, then laterally towards the vertical wicks and upwards through them towards the evaporator section. Therefore, within $0 \leqslant x \leqslant \varphi l$ region (where φ will be established later), the liquid in the upper and lower wicks possesses two distinct velocity components, u_l in the x direction, and w_l in the z direction, since, in this region, the upper wick (evaporator) gets part of the liquid supply from the lower wick. However, the liquid will have only one velocity component, u_l, along the x direction in the $\varphi l \leqslant x \leqslant l$ section, since both upper and lower wicks act as condensers. That is over the $\varphi l \leqslant x \leqslant l$ region due to the symmetrical boundary conditions, there is no liquid exchange through the vertical wicks. In the heat pipe research performed to date, researchers have made some assumptions in modeling and analysis. An important assumption made by various researchers is that the capillary porous wick is always saturated with liquid phase working fluid and vapor flows only in the core region during the operation of the heat pipe. Hence, evaluation of the effective thermal conductivity and formulation of the capillary pressure were simplified. This assumption will be employed in the present investigation. In order to obtain the integral solutions, we will make some common assumptions which are usually made in analyzing the heat pipes. The assumptions made in this work are:

(1) Vapor and liquid flow are steady, laminar and subsonic.

(2) Transport properties for the vapor and liquid are taken as constants.

(3) The vapor injection and suction rate are uniform in the evaporator and condenser sections.

(4) The vapor velocity component in the z direction is negligible since there is no injection or suction on vertical wicks.

2.1. *Vapor phase analysis*

Any one of the internal channels can be considered as a building block for the flat heat pipe. Therefore, we will concentrate on fluid flow considerations within one of these channels (Fig. 1(c)). Once the fluid characteristics within one of the channels is determined, the fluid flow characteristics of the entire heat pipe can be easily established. In our analysis the position coordinates, velocities and pressure are non-dimensionalized by $h^2 U_{ov}/\nu_v$, h, b, U_{ov}, ν_v/h and $\rho_v U_{ov}^2$ in the vapor phase, and by $h_w^2 U_{ol}/\nu_l$, U_{ol}, $\rho_l U_{ol}^2$ in the liquid phase and the temperature is non-dimensionalized by h_{fg}/R factor, where ν_v and ν_l are the kinematic viscosities, U_{ov} and U_{ol} are the maximum vapor and liquid velocities, ρ_v and ρ_l are the vapor and liquid densities, h and b are the height and half width of the vapor space of one vapor flow channel, h_w is the thickness of the wick and R is the ideal gas constant. Based on the numerical results given by Narayana [2], Faghri [3] and Sorour *et al.* [12], a parabolic velocity profile will be used for vapor flow within the heat pipe. The dimensionless velocity distri-

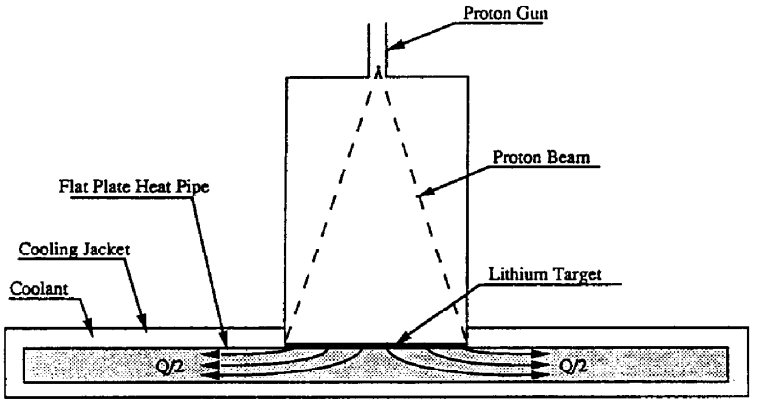

(a)

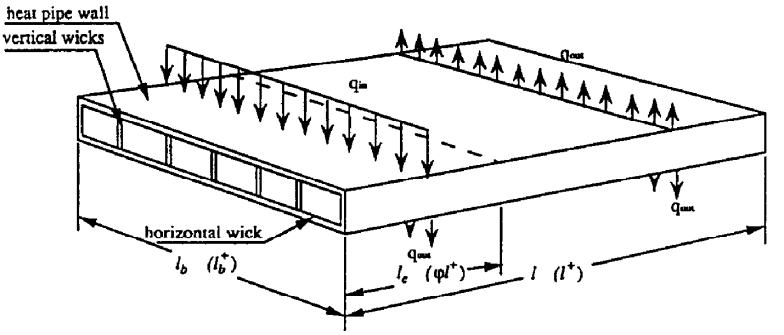

(b)

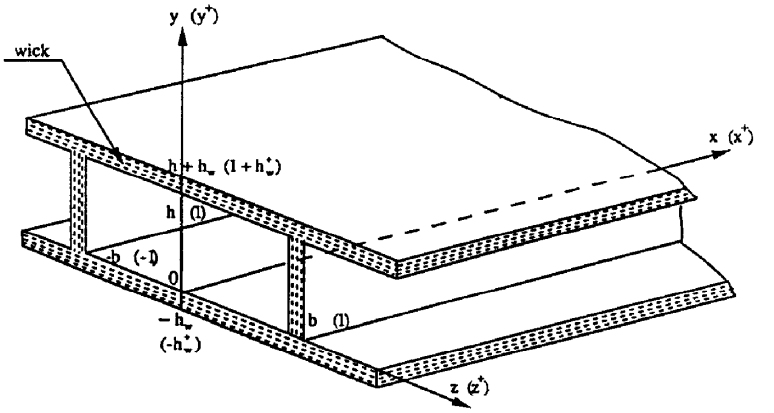

(c)

FIG. 1. Flat plate heat pipe within the BNCT system. (a) Schematic of the proposed BNCT system. (b) Parametric dimensions of the heat pipe. (c) The coordinate system used in the analysis.

bution $u_v^+(x^+, y^+, z^+)$ will be represented by a functional product in the x^+, y^+ and z^+ directions. That is

$$u_v^+(x^+, y^+, z^+) = U_v^+(x^+)[a_0 + a_1 y^+ + a_2(y^+)^2][c_0 + c_1 z^+ + c_2(z^+)^2] \quad (1)$$

where $U_v^+(x^+)$ denotes the maximum velocity for $u_v^+(x^+, y^+, z^+)$ on every transverse surface along the x^+ axis. The location of the maximum velocity will be shifted towards the lower plate due to the vapor injection from the heating side of the upper plate. Because of the symmetrical conditions in the z^+ direc-

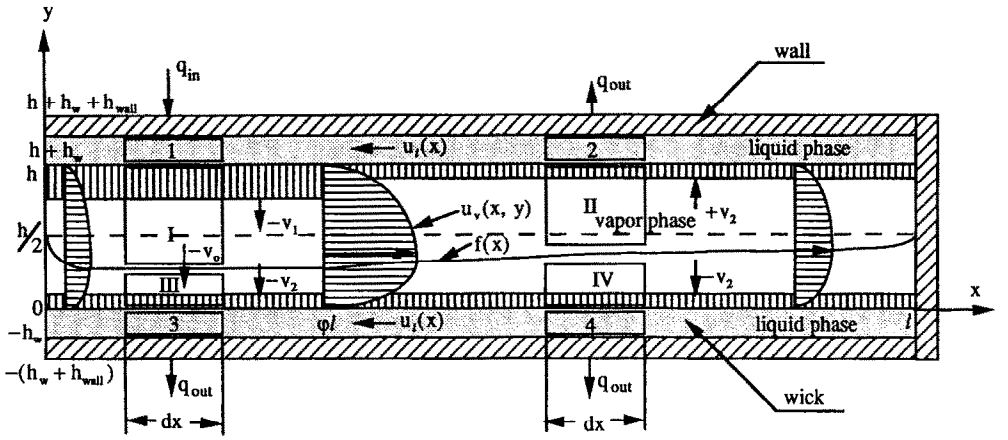

FIG. 2. Different regimes which are analyzed for the vapor and liquid phases in the x–y plane of the heat pipe.

tion (i.e. non-slip boundary conditions at $z^+ = -1$ and $z^+ = 1$), the constants c_0, c_1 and c_2 for the velocity component in the z^+ direction are easily specified as

$$[c_0 + c_1 z^+ + c_2 (z^+)^2] = [1 - (z^+)^2] \qquad (2)$$

where $z^+ = z/b$. Since the velocity component in the z^+ direction given by equation (2) is uncoupled from x^+ and y^+, the two velocity components in the x^+ and y^+ directions can be determined by concentrating only on the x^+–y^+ plane. Therefore, the velocity profile in the x^+–y^+ plane is

$$u_v^+(x^+, y^+) = U_v^+(x^+)[a_0 + a_1 y^+ + a_2 (y^+)^2]. \qquad (3)$$

Due to the asymmetry of velocity distribution in the x^+–y^+ plane, the velocity profile will be divided into two parts in the y^+ direction (Fig. 2), the lower part $(0 \leqslant y^+ \leqslant f^+(x^+))$ and the upper part $(f^+(x^+) \leqslant y^+ \leqslant 1)$, by the curve $y^+ = f^+(x^+)$, where $f^+(x^+) = f(x)/h$. The curve $y^+ = f^+(x^+)$ is the location corresponding to zero shear stress for the velocity distribution on the x^+–y^+ plane. For the lower part $(0 \leqslant y^+ \leqslant f^+(x^+))$, the boundary conditions are

$$u_v^+(x^+, 0) = 0, \quad u_v^+(x^+, f^+(x^+)) = U_v^+(x^+),$$

$$\left.\frac{\partial u_v^+(x^+, y^+)}{\partial y^+}\right|_{y^+ = f^+(x^+)} = 0.$$

Applying the above boundary conditions to equation (3) will result in the following velocity profile for the lower part

$$u_v^+(x^+, y^+) = U_v^+(x^+)\left[2\frac{y^+}{f^+(x^+)} - \left(\frac{y^+}{f^+(x^+)}\right)^2\right]$$

$$(0 \leqslant x^+ \leqslant f^+(x^+)). \qquad (4)$$

For the upper part $(f^+(x^+) \leqslant y^+ \leqslant 1)$, the boundary conditions are

$$u_v^+(x^+, 1) = 0, \quad u_v^+(x^+, f^+(x^+)) = U_v^+(x^+),$$

$$\left.\frac{\partial u_v^+(x^+, y^+)}{\partial y^+}\right|_{y^+ = f^+(x^+)} = 0.$$

The use of the above boundary conditions in equation (3) will result in the following profile for the upper part

$$u_v^+(x^+, y^+) = U_v^+(x^+)\left[2\left(\frac{1-y^+}{1-f^+(x^+)}\right) - \left(\frac{1-y^+}{1-f^+(x^+)}\right)^2\right]$$

$$(f^+(x^+) \leqslant y^+ \leqslant 1). \qquad (5)$$

To obtain the complete velocity distribution, the two unknowns $U_v^+(x^+)$ and $f^+(x^+)$ in equations (4) and (5) must be determined. First, $U_v^+(x^+)$ is determined by integrating the continuity equation with respect to y^+ from 0 to 1, i.e.

$$\int_0^1 \left(\frac{\partial u_v^+}{\partial x^+} + \frac{\partial v_v^+}{\partial y^+}\right) dy^+ = \int_0^{f^+(x^+)} \left(\frac{\partial u_v^+}{\partial x^+} + \frac{\partial v_v^+}{\partial y^+}\right) dy^+ + \int_{f^+(x^+)}^1 \left(\frac{\partial u_v^+}{\partial x^+} + \frac{\partial v_v^+}{\partial y^+}\right) dy^+ = 0. \qquad (6)$$

Substituting equation (4) into the first part of the right hand side of equation (6) (lower part $(0 \leqslant y^+ \leqslant f^+(x^+))$ and equation (5) into the second part of the right hand side of equation (6) (upper part $(f^+(x^+) \leqslant y^+ \leqslant 1)$. Also noting that in the $0 \leqslant x^+ \leqslant \varphi l^+$ section, $u_v^+(x^+, 0) = 0$, $u_v^+(x^+, 1) = 0$, $v_v^+(y^+ = 0) = -v_2^+$ and $v_v^+(y^+ = 1) = -v_1^+$, and in the $\varphi l^+ \leqslant x^+ \leqslant l^+$ section, $u_v^+(x^+, 0) = 0$ and $u_v^+(x^+, 1) = 0$, $v_v^+(y^+ = 0) = -v_2^+$ and $v_v^+(y^+ = 1) = +v_2^+$ will result the final expression for $U_v^+(x^+)$

$$U_v^+(x^+)=\begin{cases}\dfrac{3(v_1^+-v_2^+)}{2}x^+ & (0\leqslant x^+\leqslant \varphi l^+)\\ -3v_2^+(x^+-l^+) & (\varphi l^+\leqslant x^+\leqslant l^+).\end{cases}\quad(7)$$

To obtain the above equation, equation (6) is used once for the $0\leqslant x^+\leqslant\varphi l^+$ section and once for the $\varphi l^+\leqslant x^+\leqslant l^+$ section subject to proper boundary conditions. As expected, $U_v^+(x^+)$ is related to vapor injection and suction velocities. Recognizing the fact that at $x^+=\varphi l^+$, $U_v^+(x^+)$ must be continuous will result

$$\varphi=\frac{2v_2^+}{v_1^++v_2^+}.\quad(8)$$

This relation can also be obtained through a mass balance on the whole vapor space and therefore is independent of the velocity profile. Using the relation (8) and the definition of the dimensionless transverse velocity $v_1^+=v_1h/\nu_v$ as the injection Reynolds number Re_h, where v_1 is related to the input power through $v_1=Q/\rho_vA_eh_{fg}$, equation (7) can be written as

$$U_v^+(x^+)=\begin{cases}\dfrac{3(1-\varphi)Re_h}{(2-\varphi)}x^+ & (0\leqslant x^+\leqslant\varphi l^+)\\ -\dfrac{3\varphi Re_h}{(2-\varphi)}(x^+-l^+) & (\varphi l^+\leqslant x^+\leqslant l^+).\end{cases}\quad(9)$$

The $f^+(x^+)$ will be determined by integrating the x^+-momentum equation with respect to y^+ for either the lower or upper part of the heat pipe. This is because the integration of the momentum equation for the upper or the lower part in the x^+–y^+ plane produces identical results. It should be noted that in the $0\leqslant x^+\leqslant\varphi l^+$ region, there is mass flow crossing the interface between the two control volumes I and III in the vapor phase (Fig. 2) due to the vapor injector from the upper wick and suction from the lower wick. However, in the $\varphi l^+\leqslant x^+\leqslant l^+$ region, due to the symmetrical boundary conditions on both upper and lower wicks, there is no mass exchange between the two control volumes II and IV. Since the longitudinal length is much larger than the transverse length in a heat pipe, the axial sheer stress will be neglected [2, 3]. The above mentioned considerations will result in the following set of equations for the lower part of the vapor space

$$\frac{d}{dx^+}\int_0^{f^+(x^+)}(u_v^+(x^+,y^+))^2\,dy^+ - U_v^+(x^+)\frac{d}{dx^+}\int_0^{f^+(x^+)}u_v^+(x^+,y^+)\,dy^+ - U_v^+(x^+)v_2^+ = -\int_0^{f^+(x^+)}\frac{\partial p_v^+}{\partial x^+}dy^+ + \int_0^{f^+(x^+)}\frac{\partial^2u_v^+(x^+,y^+)}{\partial(y^+)^2}dy^+\quad(0\leqslant x^+\leqslant\varphi l^+).$$

$$\frac{d}{dx^+}\int_0^{f^+(x^+)}(u_v^+(x^+,y^+))^2\,dy^+ - (U_v^+(x^+))^2\frac{df^+(x^+)}{dx^+} = -\int_0^{f^+(x^+)}\frac{\partial p_v^+}{\partial x^+}dy^+ + \int_0^{f^+(x^+)}\frac{\partial^2u_v^+(x^+,y^+)}{\partial(y^+)^2}dy^+\quad(\varphi l^+\leqslant x^+\leqslant l^+).\quad(10)$$

Using the vapor velocity profile (equation (4)) and the average vapor pressure in each transverse direction in equation (10) will result

$$\frac{df^+(x^+)}{dx^+}=\begin{cases}\left\{\left[\dfrac{3(1-\varphi)Re_h}{(2-\varphi)}f^+(x^+)+\dfrac{5}{f^+(x^+)}-\dfrac{\varphi Re_h}{3(2-\varphi)}\right]\dfrac{(1-\varphi)Re_h}{(2-\varphi)}x^+ + \dfrac{f^+(x^+)}{9}\dfrac{dp^+(x^+)}{dx^+}\right\}\left[\dfrac{(2-\varphi)}{(1-\varphi)Re_hx^+}\right]^2 & (0<x^+\leqslant\varphi l^+)\\ \left\{\left[-\dfrac{16\varphi Re_h}{(2-\varphi)}f^+(x^+)+\dfrac{10}{f^+(x^+)}\right]\dfrac{\varphi Re_h}{(2-\varphi)}(l^+-x^+) + \dfrac{f^+(x^+)}{9}\dfrac{dp^+(x^+)}{dx^+}\right\}\left[\dfrac{(2-\varphi)}{\varphi Re_h(l^+-x^+)}\right]^2 & (\varphi l^+\leqslant x^+<l^+).\end{cases}\quad(11)$$

Since $U_v^+(0)=U_v^+(l^+)=0$, and the velocity distributions at $x^+=0$ and $x^+=l^+$ are uniform, the boundary conditions for the function $f^+(x^+)$ are taken as $f^+(0)=f^+(l^+)=\frac{1}{2}$. The use of equations (2), (4), (5), (9) and (11) in equation (1) will provide us with the complete velocity profile within the flat heat pipe assembly.

To obtain the pressure distribution in the vapor phase, the integrated x^+-momentum equation will be used. Integrating the x^+-momentum equation within a channel bounded by porous wicks results in the following equation in which $i=1$ corresponds to the evaporator section and $i=2$ corresponds to the condenser section

$$\int_0^{x^+}\int_0^1\int_{-1}^1\frac{\partial(u_v^+)^2}{\partial x^+}dx^+\,dy^+\,dz^+ + \int_0^{x^+}\int_0^1\int_{-1}^1\frac{\partial(u_v^+v_i^+)}{\partial y^+}dx^+\,dy^+\,dz^+ = \int_0^{x^+}\int_0^1\int_{-1}^1\left[-\frac{\partial p_v^+}{\partial x^+}+\left(\frac{\partial^2u_v^+}{\partial(y^+)^2} + \frac{1}{(h_b^+)^2}\frac{\partial^2u_v^+}{\partial(z^+)^2}\right)\right]dx^+\,dy^+\,dz^+.$$

$$i = 1, 2 \quad (0 \leqslant x^+ \leqslant l^+) \tag{12}$$

Introducing equations (2), (4), (5), (9) and (11) into equation (12) and considering the average vapor pressure at each cross-section, and carrying out the integration will result

$$\Delta p_v^+(x^+) =$$

$$\begin{cases} -\dfrac{4(1-\varphi)}{(2-\varphi)} Re_h \left\{ \left[\dfrac{16(1-\varphi)}{25(2-\varphi)} Re_h + \dfrac{1}{2(h_b^+)^2} \right] (x^+)^2 \right. \\ \left. + \displaystyle\int_0^{x^+} \frac{x^+}{f^+(x^+)(1-f^+(x^+))} \mathrm{d}x^+ \right\} \\ \qquad (0 \leqslant x^+ \leqslant \varphi l^+) \\ \Delta p(\varphi l^+) - \dfrac{4\varphi}{(2-\varphi)} Re_h \left\{ \left[\dfrac{16}{25} \dfrac{\varphi}{(2-\varphi)} Re_h \right. \right. \\ \left. - \dfrac{1}{2(h_b^+)^2} \right] [(x^+ - l^+)^2 - (\varphi l^+ - l^+)^2] \\ \left. - \displaystyle\int_0^{x^+} \frac{x^+ - l^+}{f^+(x^+)(1-f^+(x^+))} \mathrm{d}x^+ \right\} \\ \qquad (\varphi l^+ \leqslant x^+ \leqslant l^+). \end{cases} \tag{13}$$

The numerical solutions for the coupled equations, pressure $\Delta p_v^+(x^+)$ and $f^+(x^+)$, are then obtained through an iterating procedure involving equations (11) and (13). An approximate solution for the $f^+(x^+)$ can be found if Bernoulli's equation is used at $y^+ = f^+(x^+)$. This will result

$$\frac{\mathrm{d}f^+(x^+)}{\mathrm{d}x^+} =$$

$$\begin{cases} \left[-\dfrac{9}{2}(1-\varphi) f^+(x^+) + 5 \dfrac{(2-\varphi)}{Re_h} \dfrac{1}{f^+(x^+)} \right. \\ \left. - \dfrac{5}{2}\varphi \right] \dfrac{1}{(1-\varphi)x^+} \\ \qquad (0 < x^+ \leqslant \varphi l^+) \\ \left[-\varphi f^+(x^+) + 10 \dfrac{(2-\varphi)}{Re_h} \dfrac{1}{f^+(x^+)} \right] \dfrac{1}{7\varphi(l^+ - x^+)} \\ \qquad (\varphi l^+ \leqslant x^+ < l^+). \end{cases} \tag{14}$$

The above approximate solution for $f^+(x^+)$ is used as the initial guess in our iterative numerical scheme.

2.2. *Liquid phase analysis*

Within the thin porous wick, Darcy's law will be applied. The dimensionless Darcy's law is

$$\frac{\partial p_l^+}{\partial x^+} = \frac{1}{K^+} u_l^+ \tag{15}$$

where $K^+ = K/h_w^2$. It should be noted that the boundary and inertia effects are neglected in this work [13].

From Fig. 2, it can be seen that the liquid velocity u_l^+ is related to both vapor injection and suction velocities. Adding the lower and upper wick mass conservation equations for the section $0 \leqslant x^+ \leqslant \varphi l^+$ to cancel out w_l^+ in z^+ direction will result in the following one-dimensional velocity distribution in the x^+ direction

$$2 \frac{\mathrm{d}}{\mathrm{d}x^+}(u_l^+(x^+)) = h_w^+ \mu^+ (v_1^+ - v_2^+) \quad (0 \leqslant x^+ \leqslant \varphi l^+) \tag{16}$$

where $\mu^+ = \mu_v/\mu_l$ and $h_w^+ = h_w/h$. While for the $\varphi l^+ \leqslant x^+ \leqslant l^+$ section, we obtain

$$\frac{\mathrm{d}}{\mathrm{d}x^+}(u_l^+(x^+)) = -h_w^+ \mu^+ v_2^+ \quad (\varphi l^+ \leqslant x^+ \leqslant l^+). \tag{17}$$

Subject to the boundary conditions

$$u_l^+(0) = u_l^+(l^+) = 0$$

the above equations provide the liquid phase velocity distribution as

$$u_l^+(x^+) = \begin{cases} \dfrac{h_w^+ \mu^+ (v_1^+ - v_2^+)}{2} x^+ & (0 \leqslant x^+ \leqslant \varphi l^+) \\ h_w^+ \mu^+ v_2^+ (l^+ - x^+) & (\varphi l^+ \leqslant x^+ \leqslant l^+). \end{cases} \tag{18}$$

At $x^+ = \varphi l^+, u_l^+(x^+)$ given by both sides of the above equation should be equal. This gives the value for φ as

$$\varphi = \frac{2v_2^+}{v_1^+ + v_2^+}.$$

As expected, this is the same as the result obtained from the vapor phase analysis (equation (8)). The pressure distribution in the wick in the x^+ direction is obtained by substituting equation (18) into Darcy's law, equation (15). This will result

$$\Delta p_l^+(x^+) =$$

$$\begin{cases} \displaystyle\int_0^{x^+} \frac{h_w^+ \mu^+}{K^+} \frac{(v_1^+ - v_2^2)}{2} x^+ \mathrm{d}x^+ & (0 \leqslant x^+ \leqslant \varphi l^+) \\ \displaystyle\int_{\varphi l^+}^{x^+} \frac{h_w^+ \mu^+}{K^+} v_2^+ (l^+ - x^+) \mathrm{d}x^+ & (\varphi l^+ \leqslant x^+ \leqslant l^+). \end{cases} \tag{19}$$

The boundary condition for equation (19) is obtained by using the following physical assumption [5, 6, 11, 14]

$$\Delta p_l^+(l^+) = \Delta p_v^+(l^+).$$

Integrating (19) subject to the above boundary condition results in the pressure distribution in the liquid phase

$$\Delta p_l^+(x^+) =$$

$$\begin{cases} \Delta p_v^+(l^+) - \dfrac{h_w^+ \mu^+ (1-\varphi) Re_h}{2(2-\varphi)K^+}\{\varphi(1-\varphi)(l^+)^2 \\ \quad +[(\varphi l^+)^2 - (x^+)^2]\} \quad (0 \leqslant x^+ \leqslant \varphi l^+) \\ \Delta p_v^+(l^+) \\ \quad - \dfrac{h_w^+ \mu^+ \varphi Re_h}{2(2-\varphi)K^+}(l^+ - x^+)^2 \quad (\varphi l^+ \leqslant x^+ \leqslant l^+). \end{cases} \tag{20}$$

2.3. *Temperature distribution*

Once the vapor pressure distribution is found, the vapor temperature distribution can be specified by using the Clausius–Clapeyron equation. In this work, the vapor is assumed to behave as an ideal gas and the volume of the liquid within the vapor phase is neglected [6, 12]. The dimensionless temperature profile based on the Clausius–Clapeyron equation can be found from

$$\Delta T_v^+(x^+) = (T_{ov}^+)^2 \left[\frac{\ln p_w^+ 2(x^+) - \ln p_{ov}^+}{1 - T_{ov}^+(\ln p_{ov}^+ - \ln p_v^+(x^+))} \right] \tag{21}$$

where $T_{ov}^+(x^+) = T_{ov}(h_{fg}/R)$ is the dimensionless saturated vapor temperature.

2.4. *Operational criteria*

In general, the operational limits which need to be satisfied for a heat pipe under steady state and low temperature situations [5] are usually based on the boiling and capillary limit criteria. First, the capillary operational limit is established. To satisfy the capillary limit, the maximum capillary pressure head $(\Delta p_{cap})_{max}$ must be greater than the total vapor, liquid and gravitational pressure drops [5, 10, 11]. That is

$$(\Delta p_{cap})_{max} \geqslant \Delta p_{total} \tag{22}$$

where

$$\Delta p_{total} = \Delta p_v + \Delta p_l + \Delta p_g.$$

The gravitational head Δp_g can be neglected for the horizontal heat pipe, and the overall vapor and liquid pressure drops are established as

$$\Delta p_v = p_v(0) - p_v(l)$$
$$\Delta p_l = p_l(l) - p_l(0). \tag{23}$$

Therefore, the total pressure head is presented as

$$\Delta p_{total} = \Delta p_v + \Delta p_l = p_v(0) - p_l(0). \tag{24}$$

The total capillary pressure head along the heat pipe is given by

$$\Delta p_{cap} = 2\sigma\left(\frac{\cos\theta_c}{r_{w,e}} - \frac{\cos\theta_c}{r_{w,c}}\right).$$

Based on Tien [5], Dunn and Reay [10], Ivanovskii *et al.* [11] and Chisholm [14] the wetting angle between the liquid and wick in the evaporator section is $\theta_e = 0$ whereas in the condenser section this wetting angle is $\theta_c = \pi/2$. Therefore the maximum capillary pressure head of Δp_{cap} can be written as

$$(\Delta p_{cap})_{max} = \frac{2\sigma_l}{r_w} \tag{25}$$

where σ_l denotes the surface tension of the liquid in the wick, and r_w is the porous radius of the wick. Using the results given by equations (13) and (20), we will show in the next section that the operational criterion for the heat pipe is indeed established. In what follows it will be shown that the boiling limit criterion is also satisfied. For a water heat pipe near atmospheric pressure, the critical heat flux for boiling limit is of the order of 10^8 W m^{-2}. However, for our case, the critical heat flux is [5]

$$q_{boil} = \frac{h_{fg} p_o}{\sqrt{(2\pi RT)}} \exp\left(-\frac{h_{fg}}{RT}\right) = 1.06 \times 10^7 \text{ W m}^{-2}$$

which is almost an order of magnitude higher than the maximum heat flux imposed on the heat pipe. Therefore, both the capillary and boiling limit criteria are satisfied for high heat flux situations such as the BNCT application.

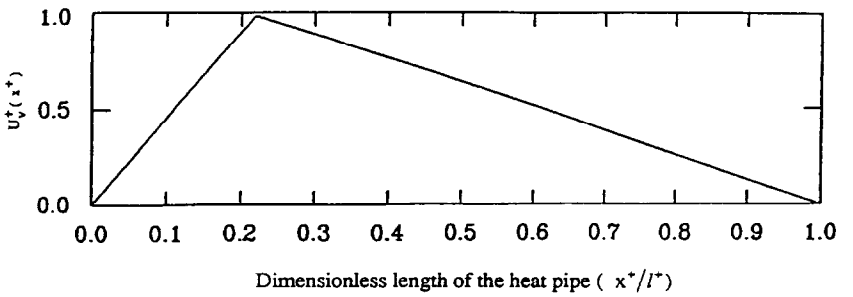

FIG. 3. Variations of $U_v^+(x^+)$ vs x^+/l^+.

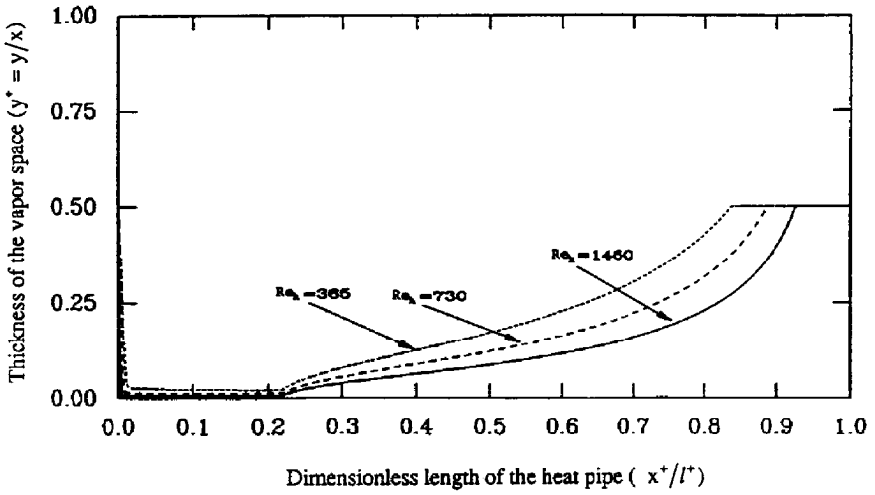

FIG. 4. Variations of $f^+(x^+)$ for different values of injection Reynolds number, Re_h.

3. RESULTS AND DISCUSSION

The results presented here are based on a flat heat pipe with heavy water as the working fluid. The pipe dimensions based on our application (see Fig. 1(b)) are chosen as: $l = 0.46$ m, $l_h = 0.25$ m, $b = 0.0125$ m, and $h = 0.0254$ m. The evaporator section, $l_e = 0.101$ m, is only on the top surface of the heat pipe.

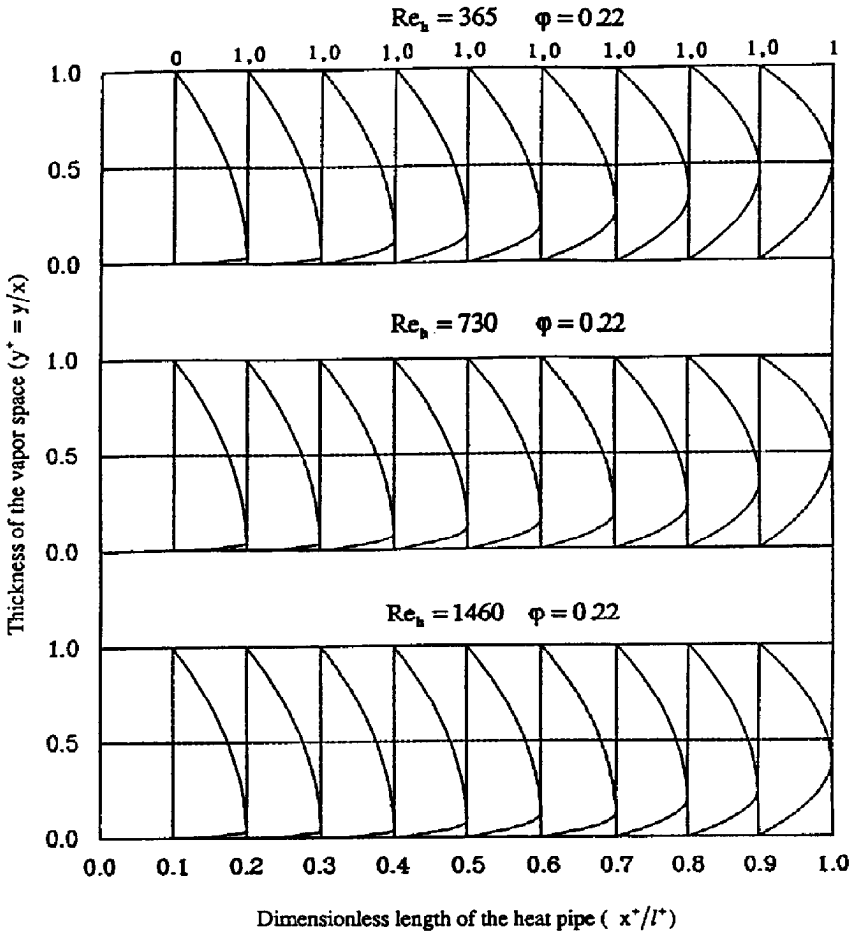

FIG. 5(a). Effects of the injection Reynolds number on the velocity distributions ($z' = 0$).

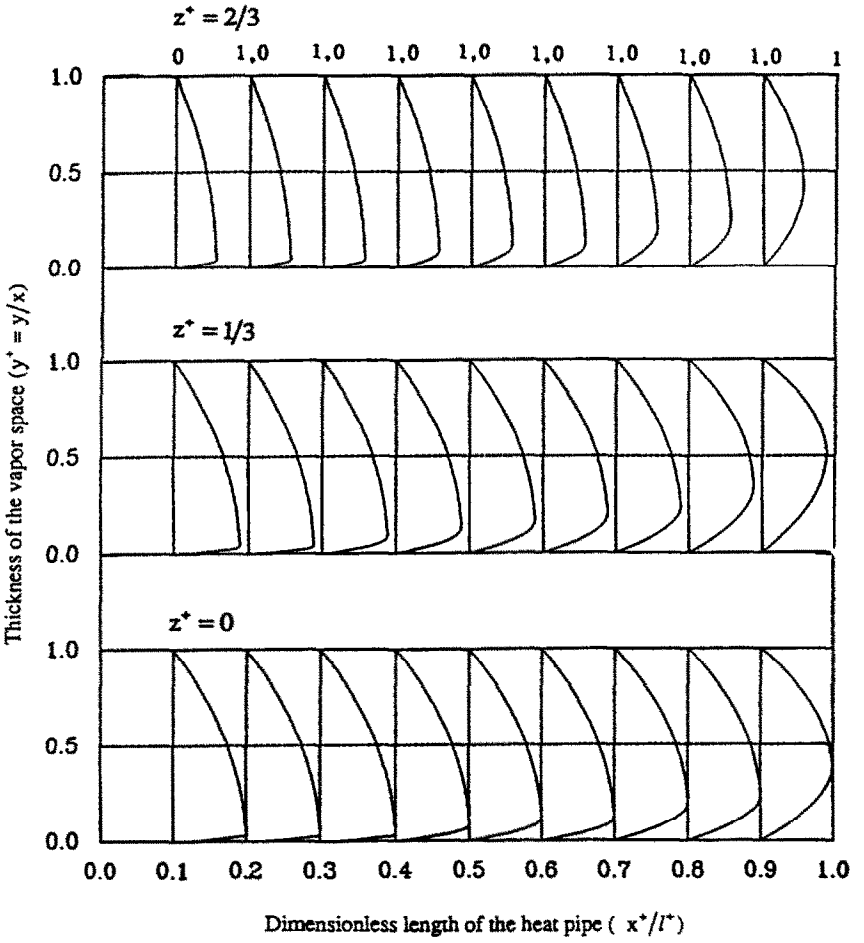

FIG. 5(b). The velocity distributions at different lateral locations for $Re_h = 1460$.

The rest of the heat pipe's external area acts as the condenser section. The maximum heat flux at the evaporator section of the heat pipe can then be calculated as

$$q_e = \frac{Q}{A_e} = 1.8293 \times 10^6 \text{ W m}^{-2} = 182.93 \text{ W cm}^{-2}. \tag{26}$$

Since the light water will hamper the traverse of neutrons, heavy water (D_2O), which has almost the same thermophysical properties except having a larger density than light water, is chosen as the working fluid for the heat pipe. The material for the container and the wick is chosen to be aluminum. The heat pipe must be designed such that the lithium target will be solid at all times. Since the melting temperature for lithium is 180°C, the target will remain solid if the vapor temperature is controlled at $T_{vapor} = 80°C$. This can be seen through examination of the corresponding lithium temperature

$$T_{Li} = T_{vapor} + \Delta T_{wick} + \Delta T_{wall} + \Delta T_{Li} < 180°C \tag{27}$$

where

$$\Delta T_{wick} = q_e \frac{h_w}{k_{wick}} = 32.9°C$$

$$\Delta T_{wall} = q_e \frac{h_{wall}}{k_{wall}} = 15.5°C$$

$$\Delta T_{Li} = q_e \frac{h_{Li}}{k_{Li}} = 42.7°C$$

and where $h_{Li} = 1 \times 10^{-3}$ m, $h_{wall} = 2 \times 10^{-3}$ m and $h_w = 2 \times 10^{-3}$ m are the thicknesses of lithium target, the container wall and the wick, respectively, and $k_{Li} = 42.8$ W m^{-1} °C^{-1}, $k_{wall} = 236$ W m^{-1} °C^{-1} and $k_{wick} = 94.65$ W m^{-1} °C^{-1} are thermal conductivities of the lithium, aluminum and the wick, respectively. Based on the above calculations, the vapor temperature should be less than 88.9°C to satisfy equation (27). Therefore, the operating vapor temperature is chosen to be 80°C to ensure that there will be no phase change in the lithium layer.

The thermophysical properties of the heavy water used in our calculations (at $T_v = 80°C$) are: $h_{fg} = 2128$ kJ kg^{-1}, $\mu_l = 1.1876 \times 10^{-5}$ Ns m^{-2}, $\mu_v = 41.6 \times 10^{-5}$ Ns m^{-2}, $\rho_v = 0.3055$ kg m^{-3} and $\rho_l = 1078.3$ kg m^{-3}.

The saturated vapor pressure corresponding to $T_v = 80°C$ is $p_{sat} = 4.44 \times 10^4$ Pa. The imposed energy rate based on the BNCT application is $Q = 75$ kW, which will result an average injection velocity in the evaporator section

$$v_1 = \frac{Q}{A_e h_{fg} \rho_v} = 2.813 \text{ m s}^{-1}.$$

This will correspond to an injection Reynolds number of $Re_h = 1460$ for $Q = 75$ kW. As seen from equations (9), (11), (13), (18), (20), the $f^+(x^+)$ and non-dimensional velocity and pressure distributions for both the vapor and liquid phases are functions of two pertinent parameters. These are: Re_h, which represents the input power, and φ, which represents the geometric ratio of the length of evaporator to the entire length of the heat pipe. Equations (11) and (13) were solved by using a standard Runge–Kutta method. The numerical results for functions $U_v^+(x^+)$, $f^+(x^+)$, vapor velocity distributions $u_v^+(x^+, y^+, z^+)$ at different z^+ locations, average vapor and liquid pressure distributions and the average vapor temperature distribution are shown on Figs. 3–7.

Figure 3 demonstrates the variation of $U_v^+(x^+)$ along the x^+ axis. It can be seen that $U_v^+(x^+)$ increases in the $0 \leqslant x^+ \leqslant \varphi l^+$ region corresponding to the evaporator section and decreases in the $\varphi l^+ \leqslant x^+ \leqslant l^+$ region corresponding to the condenser section due to the vapor injection (increasing mass) and suction (decreasing mass) over the corresponding regions. This variation of $U_v^+(x^+)$ is linear because of uniform vapor injection and suction velocities. This behavior is similar to the results reported by Bankston and Smith [4].

Figure 4 illustrates the functional distribution for $f^+(x^+)$, which represents the location for the maximum value of $u_v^+(x^+, y^+)$, at different injection Reynolds numbers. It can be seen that right after $x^+ > 0$, the maximum velocity is profoundly shifted towards the cooling side. As expected for larger values of Re_h, the maximum vapor velocity will be shifted more prominently towards the cooling side, and it also takes a longer length before $f^+(x^+)$ approaches

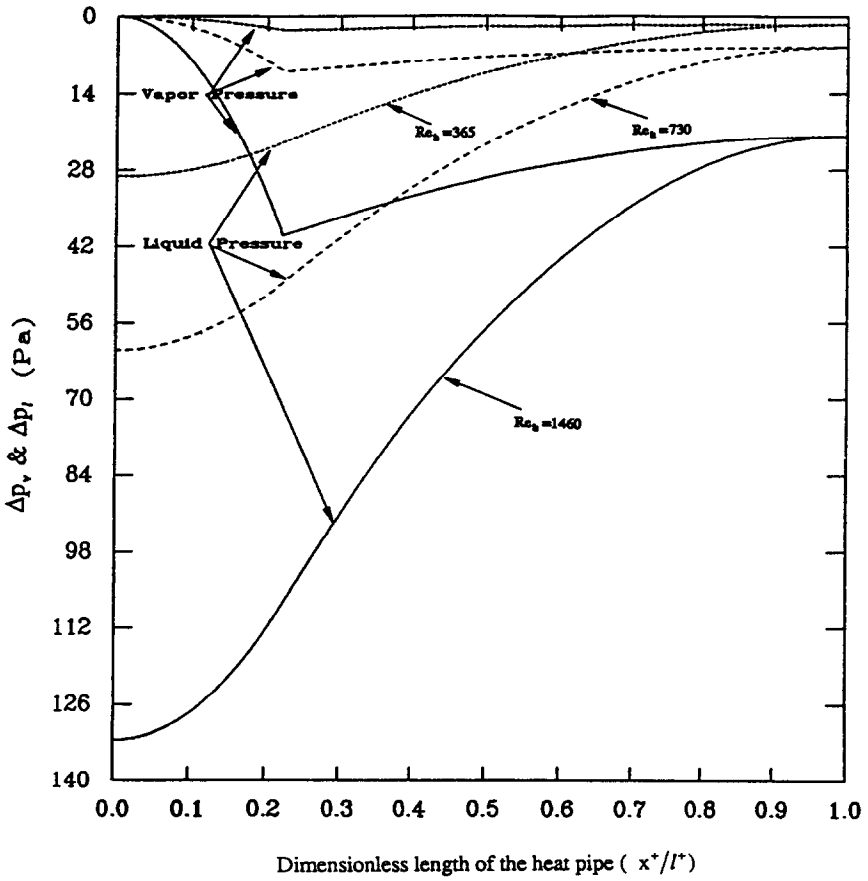

FIG. 6. Vapor and liquid pressure distributions along the heat pipe.

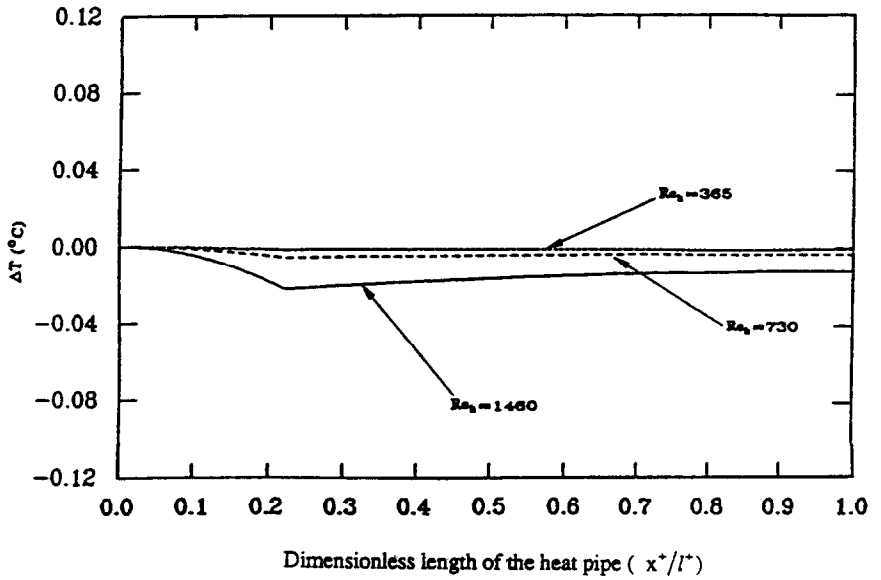

FIG. 7. Vapor temperature profiles for different injection Reynolds numbers.

the center line. Figure 5(a) clearly shows that for smaller Reynolds numbers, the symmetrical transition of the velocity profile will occur earlier. Figure 5(b) shows the x^+–y^+ velocity distribution at different lateral locations for $Re_h = 1460$.

To obtain a better feel for the operational criterion, the solutions for the pressure and temperature distributions are presented dimensionally. Figure 6 presents the vapor and liquid pressure distributions along the heat pipe at different Reynolds numbers. These profiles show the effects of the pressure head loss in the evaporator region due to vapor velocity acceleration in that region, and the pressure head recovery in the condenser region due to the deceleration of the vapor velocity in that region. In the liquid phase, there is only pressure head loss, since the flow is dominated by the bulk frictional resistance from the porous matrix. As expected, the smaller the Reynolds number, the smaller the pressure head loss. The qualitative behavior of the overall pressure distribution along the heat pipe is quite close to results presented by Tien and Rohani [1], Winter and Barsch [6], Dunn and Reay [10] and Ivanovskii *et al.* [11]. Figure 6 demonstrates the variations for the mean vapor temperature along the longitudinal direction at different injection Reynolds numbers. It can be seen that the temperature is quite uniform ($\Delta T \ll 1$°C), even for the highest input power ($Re_h = 1460$). This is consistent with the numerical and experimental results reported by Chen and Faghri [15]. This further demonstrates the successful operation of the heat pipe [6].

Finally, the capillary operational criterion for the heat pipe can be contrasted from the numerical results given on Fig. 6. The total pressure drop in the heat pipe is

$$\Delta p_{\text{total}} = 133\,\text{Pa}$$

corresponding to $Re_h = 1460$ ($Q = 75$ kW). Using equation (25) results

$$(\Delta p_{\text{cap}})_{\max} = \frac{2\sigma_l}{r_w} = 545\,\text{Pa}.$$

Obviously, $(\Delta p_{\text{cap}})_{\max} > \Delta p_{\text{total}}$. Thus the capillary operational criterion for the heat pipe under the design conditions dictated by the BNCT application is also satisfied.

4. CONCLUSIONS

An in-depth integral analysis for an asymmetrical flat plate heat pipe is presented in this work. Analytical results for the shifted vapor velocity profiles on the x–y plane, the overall axial pressure distributions in both vapor and liquid phases and the axial vapor temperature distribution in the heat pipe are obtained. The feasibility and the pertinent operational criteria for using the flat plate heat pipe for high heat flux situations such as the BNCT application were also investigated and it has been shown that the heat pipe can be used as an effective heat sink for removal of the heat generated from proton bombardments of a lithium target as well as an additional moderator for the neutron production.

Acknowledgements—This work was supported by the Department of Energy under contract number DE-FGO2-89ER60872. The authors would like to thank Dr Thomas Blue for his help on this work.

REFERENCES

1. C. L. Tien and A. R. Rohani, Analysis of the effect of vapor pressure drop on heat pipe performance, *Int. J. Heat Mass Transfer* **17**, 61–67 (1974).
2. K. B. Narayana, Vapor flow characteristics of slender

cylindrical heat pipes—a numerical approach, *Numer. Heat Transfer* **10,** 79–93 (1986).
3. A. Faghri, Vapor flow analysis in a double-walled concentric heat pipe, *Numer. Heat Transfer* **10,** 583–595 (1986).
4. C. A. Bankston and H. J. Smith, Vapor flow in cylindrical heat pipes, *J. Heat Transfer* **95,** 371–376 (1973).
5. C. L. Tien, Fluid mechanics of heat pipes, *Ann. Rev. Fluid Mech.* **7,** 167–185 (1975).
6. E. R. F. Winter and W. O. Barsch, The heat pipe, *Adv. Heat Transfer* **7,** 219–320 (1971).
7. K. S. Udell, Heat transfer in porous media considering phase change and capillarity—the heat pipe effect, *Int. J. Heat Mass Transfer* **28,** 485–495 (1985).
8. I. Fatt and W. A. Klikoff, Effect of fractional wettability on multiphase flow through porous media, *AIME Trans.* **216,** 256 (1959).
9. K. S. Udell and J. S. Fitch, Heat transfer in porous media and particulate flows, *ASME HTD* **46,** 103–110 (1985).
10. P. D. Dunn and D. A. Reay, *Heat Pipes*, 3rd Edn, Chapter 2. Pergamon Press, New York (1982).
11. M. N. Ivanovskii, V. P. Sorokin and I. V. Yagodkin, *The Physical Principles of Heat Pipes*, Chapters 1, 2. Clarendon Press, Oxford (1982).
12. M. M. Sorour, M. A. Hassab and S. Estafanous, Developing laminar flow in a semi-porous two dimensional channel with nonuniform transpiration, *Int. J. Heat Fluid Flow* **8,** 44–53 (1987).
13. K. Vafai, Convective flow and heat transfer in variable porosity media, *J. Fluid Mech.* **147,** 233–259 (1984).
14. D. Chisholm, *The Heat Pipe*, Chapter 2. Mill & Boon, London (1971).
15. M. M. Chen and A. Faghri, An analysis of the vapor flow and the heat conduction through the liquid-wick and pipe wall in a heat pipe with single or multiple heat sources, *Int. J. Heat Mass Transfer* **33,** 1945–1955 (1990).

ANALYSE DES CARACTERISTIQUES D'ECOULEMENT ET DE TRANSFERT DE CHALEUR D'UN CALODUC ASYMETRIQUE PLAT

Résumé—Une analyse intégrale en profondeur révèle différents aspects physiques d'un caloduc asymétrique plat. Le champ pseudo-tridimensionnel d'écoulement de la phase vapeur est bifurqué sur le plan x–y à cause de la nature disymétrique des sources et des puits de chaleur. Les résultats pour les profils de vitesse en x–y, les distributions axiales de pression dans les phases vapeur et liquide et la distribution axial de la température de la vapeur sont obtenus. Il y a un bon accord qualitatif entre les résultats présentés et ceux basés sur la résolution du cas symétrique conventionnel. L'analyse fournit des expressions analytiques précises pour les distributions de vitesse et de pression dans le type non conventionnel de caloduc.

UNTERSUCHUNG VON STRÖMUNG UND WÄRMEÜBERGANG IN EINEM ASYMMETRISCHEN PLATTENFÖRMIGEN WÄRMEROHR

Zusammenfassung—In der vorliegenden Arbeit werden die unterschiedlichen physikalischen Gesichtspunkte eines asymmetrischen plattenförmigen Wärmerohres eingehend untersucht. Es ergibt sich ein pseudo-dreidimensionales Strömungsfeld für den Dampf, das wegen der asymmetrischen Art von Wärmequelle und Wärmesenke in der x–y Ebene dargestellt wird. Die analytischen Ergebnisse für die verschobenen Geschwindigkeitsprofile für den Dampf in der x–y Ebene, die Druckverteilungen in axialer Richtung für Dampf und Flüssigkeit sowie die axiale Verteilung der Dampftemperatur im Wärmerohr werden ermittelt. Die vorgestellten Ergebnisse und die Ergebnisse aufgrund der Lösung der Feldgleichungen für den herkömmlichen symmetrischen Fall stimmen qualitativ gut überein. Es ergeben sich genaue analytische Ausdrücke für die Verteilungen von Geschwindigkeit und Druck in dem betrachteten nichtherkömmlichen Wärmerohr.

АНАЛИЗ ХАРАКТЕРИСТИК ТЕЧЕНИЯ И ТЕПЛОПЕРЕНОСА В АСИММЕТРИЧНОЙ ПЛОСКОЙ ТЕПЛОВОЙ ТРУБЕ

Аннотация—Подробно анализируются различные физические характеристики асимметричной плоской тепловой трубы. Образующееся псевдотрехмерн поле течения пара разветвляется в плоскости x–y в силу асимметричности теплового источника и стоков. Получены аналитические результаты для профилей скоростей пара в плоскости x–y, аксиальных распределений давления в парообразной и жидкой фазах, а также аксиального распределения температур пара. Результаты качественно согласуются с данными, полученными при решении уравнений поля в симметричном случае.